Evaluation of Simulator Incorporating Non-equilibrium Green's Function and Improvement of Quantum Cascade Lasers Output using the Simulator

Shigeyuki Takagi[1], Hirotaka Tanimura[1][a], Tsutomu Kakuno[2], Rei Hashimoto[2],
Kei Kaneko[2] and Shinji Saito[2]

[1]*Department of Electrical and Electronics Engineering, School of Engineering, Tokyo University of Technology,*
1404-1 Katakura-cho, Hachioji-city, Tokyo, Japan
[2]*Corporate Manufacturing Engineering Center, Toshiba Corporation, 8 Shinisogo-cho, Isogo Ward,*
Yokohama-city, Kanagawa, Japan

Keywords: Quantum Cascade Lasers, QCLs, Non-equilibrium Green's Function, Electron Scattering, Quantum Well.

Abstract: We applied a simulator incorporating a non-equilibrium Green's function (NEGF) to quantum cascade laser (QCL) wavelength prediction, and confirmed its validity including its temperature dependence. In addition, the electroluminescence (EL) intensity of the QCL was increased by a factor of 1.4 by including a structure that made the light-emitting layer barrier thin calculated using the simulator. The NEGF is used to calculate the electron density existing in the QCL and the laser gain. To examine the validity of wavelength calculation, we calculated the oscillation wavelengths for the seven types of film structure in the 3 to 9 μm band in our references, and compared them with the experimental results. As a result, the difference between them was well below 0.36 μm. Furthermore, the film structure for increasing the gain was calculated on the basis of the structure reported in one of the references. The gain was increased 1.17 to 1.28 times by reducing the thicknesses of the barriers by 10%. The QCLs with this film structure were prototyped and their EL output intensity was measured. It was confirmed that the EL output intensity output was improved and the film structure design obtained using the simulator was effective.

1 INTRODUCTION

Quantum cascade lasers (QCLs) are n-type semiconductor lasers in which two types of semiconductor film are alternately stacked, and the laser light in the infrared region can be obtained (Faist et al., 1994). Conventional semiconductor lasers (LDs) are limited to visible part of the spectrum and infrared wavelengths below 3 μm. QCLs oscillate in the infrared region, and the desired wavelength can be obtained simply by changing the thickness of a multilayer film using two kinds of materials.

Since the QCL wavelength is in the infrared region, QCLs are expected to be applied in trace gas analysis and remote gas detection. To realize this, a QCL with a wavelength suitable for such measurements is required. Furthermore, with such trace substance detection and remote gas detection,

higher sensitivity is expected by increasing the output. Since the amount of laser absorption is measured in the detection of trace substances, it is necessary for the laser to propagate a long optical path. To develop a laser with such a high output and a wavelength suitable for measurement, it is effective to use a simulator that can predict the oscillation wavelength and gain.

In the current simulators, the Schrödinger equation is solved to calculate the wave function, and the laser light intensity is calculated from the lifetimes of the upper and lower levels and the transition probabilities between the upper and lower levels semi-classically (Jirauschek and Kubis, 2014). On the other hand, in the calculation using a non-equilibrium Green's function (NEGF), the electron density distribution and the transition of electrons from the upper level to the lower level can be

[a] https://orcid.org/0000-0002-7653-4602

calculated quantum mechanically. Furthermore, by determining the self-energy of electron scattering, we can easily add the effect of electron scattering on the electron distribution. Not only can the gain be calculated accurately, it is also possible to reflect the effects of operating temperature and film stress.

Then, we introduced a simulator that incorporates NEGF for the calculation of electron density (Grange, 2015). Oscillation wavelengths were calculated for structures with wavelengths of 3 to 9 μm reported so far, and compared with the wavelengths actually measured in previous study. To investigate the temperature dependence of the simulator, the oscillation wavelength from 77 to 293K was calculated for a film structure QCL with an oscillation wavelength of 4 μm, and the temperature dependence was consistent with the wavelength of the prototype QCL. Furthermore, the active layer was designed to increase the gain using a simulator, and it was shown that the output could be improved by reducing the barrier of the light-emitting layer. As a result of evaluating the QCL with this structure, the EL emission intensity was increased 1.4-fold compared with the previous structure QCL, and it was shown that the simulator design method is effective for the structure design of QCLs.

2 SIMULATOR INCORPORATING NEGF

2.1 Composition of Simulator

Nextnano.QCL (Nextnano GmbH) was used for calculating the oscillation wavelength of QCLs. Figure 1 shows the calculation flow in the simulator. Assuming that the unperturbed Hamiltonian is H_o and the electron scattering is the perturbation term Hamiltonian H_{scatt} in the Schrödinger equation, the Hamiltonian H is expressed by Eq. (1).

$$H = H_o + H_{scatt} \tag{1}$$

Next, the Poisson equation is solved to find the mean-field electrostatic potential, and the retarded self-energy Σ^R and the lesser self-energy $\Sigma^<$ describing electron scattering are calculated. The density of States (DOS) is obtained from the retarded Green's function G^R using the Dyson equation shown in Eq. (2).

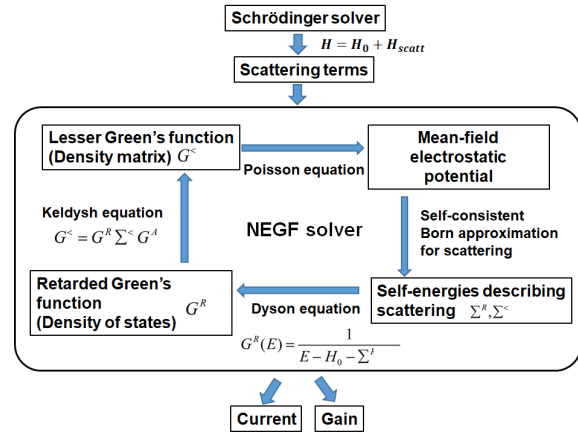$$G^R = \frac{1}{E - H_0 - \Sigma^R} \tag{2}$$

Figure 1: Calculation flow of NEGF simulator.

Using the Keldysh equation shown in Eq. (3), we obtained the electron density matrix from the lesser Green's function $G^<$,
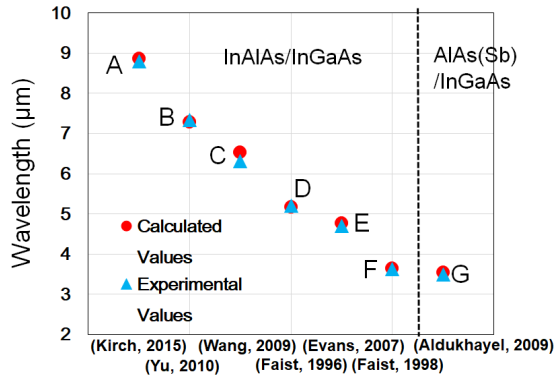
$$G^< = G^R \Sigma^< G^A , \tag{3}$$

where G^A is an advanced Green's function. In the NEGF, the above calculations are repeated until $G^<$ converges below the set threshold. That is, $G^<$ is obtained by a self-consistent method. On the basis of the obtained electron density matrix, the current and the gain of the QCL are calculated.

From a series of calculations, the relationship between the energy (wavelength) and the gain is calculated. The oscillation wavelength of the laser is determined as the wavelength that maximizes the gain. By using the NEGF, we can add the effects such as the crystal lattice and electron scattering to the simulation. In this way, it is possible to perform the calculation while taking into consideration of the influence on the film stress and electrons scattering to the crystal lattice corresponding to the operating temperature of the QCL.

2.2 Structure and Oscillation Wavelength

We selected seven papers in which oscillation in the 3 to 9 μm band was reported (Kirch et al, 2015, Yu et al., 2010, Wang et al, 2009, Faist et al., 1996, Evans et al., 2007, Faist et al., 1998, Aldukhayel et al., 2009), and the oscillation wavelength in each film structure was calculated using the simulator. The wavelengths in the references and those obtained by simulation are shown in Fig. 2. The left side of the dotted line is the material InAlAs/InGaAs, and the right side (G) is the film material AlAs(Sb) / InGaAs. The differences between the simulations and the

experiment are less than 0.4 μm except for B of 0.59 in the QCL with the film material InAlAs/InGaAs. In the case of G, the difference is 0.045 μm, and it is shown that the calculated values reproduce the experimental values well even if the film material is changed.

A: Kirch, D. et al. "Highly temperature insensitive, low threshold-current density (λ = 8.7–8.8 μm) quantum cascade lasers"
B: Yu, J S. et al. "Injector doping level-dependent continuous-wave operation of InP-based QCLs at λ ~ 7.3 μm above room temperature"
C: Wang, C. et al. "Mode-locked pulses from mid-infrared quantum cascade lasers"
D: Faist, J. et al. "High power mid-infrared (λ ~ 5 μm) quantum cascade lasers operating above room temperature"
E: Evans, A. et al. "Buried heterostructure quantum cascade lasers with high continuous-wave wall plug efficiency"
F: Faist, J. et al. "Short wavelength quantum cascade laser based on strained compensated InGaAs/AlInAs"
G: Aldukhayel, A. et al. "Investigations of carrier scattering into L-valley in λ = 3.5 μm InGaAs/AlAs(Sb) quantum cascade lasers using high hydrostatic pressure"

Figure 2: Comparison of wavelengths reported in papers and wavelengths obtained by simulation.

In parallel with the simulation, we fabricated two QCLs with an oscillation wavelength in the 4 μm band. The QCL has 30 cycles of active layers, whose structure is the same as that used by Evans et al. The device length is 4 mm and the ridge width is 12 μm.

The QCLs were operated at 100 kHz with a pulse width of 300 ns at room temperature (293 K). The oscillation wavelength of the prototype QCL is shown in Fig. 3 (a). The two prototype devices oscillated at wavelengths of 4.41 and 4.90 μm, respectively. The differences between the calculated wavelengths and the measured wavelengths, including our experimental results, are within 0.36 μm. The output characteristics of the QCL with an oscillation wavelength of 4.41 μm are shown in Fig. 3 (b). A peak output of about 400mW is obtained.
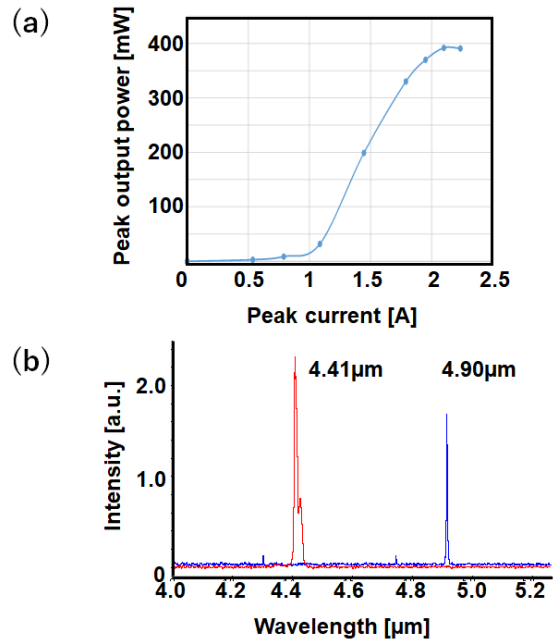

Figure 3: QCL output characteristics (a) and oscillation wavelength (b).

2.3 Temperature Dependence

To investigate the temperature dependence of the simulation results, the operating temperature was changed from 84 to 241 K in the simulation. The temperature dependence was also measured with our QCL with an oscillation wavelength of 4.41 μm fabricated as described in Sec 2.2. The simulation results were compared with the experimental results of the prototype QCL and the measurement results Wen et al., 2011) of Wen et al. The active layer structures are all the same as those used by Evans et al. The temperature ranges at which the oscillation wavelength was measured are from 84 to 241 K in the work by Wen et al. and from 77 to 294 K in our experiment.

The simulation results, our experimental results, and the results of Wen et al. are shown in Fig. 4. The oscillation wavelength of the simulation is slightly longer than those obtained by Wen et al. and with our prototype QCL. The simulation results reproduce the tendency that the wavelength increases with increasing temperature. The change in wavelength with the temperature (the tuning coefficient of the wavelength) is as follows. The tuning coefficients are 0.58 nm/K in the simulation, 0.81 in the experiment by Wen et al. and 0.50 nm/K in our experiment. The tuning coefficients in the simulations are between that obtained by Wen et al. and that obtained with our QCL, and the temperature dependence of the QCL oscillation wavelength can be well reproduced.
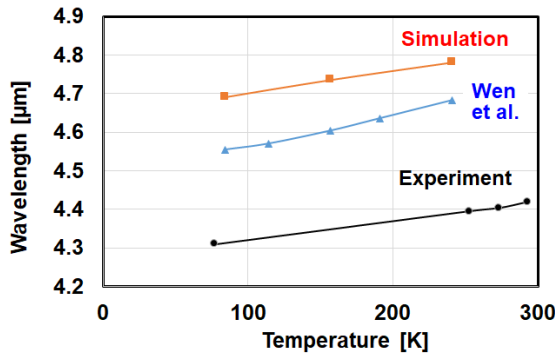
Figure 4: Wavelength dependence on operating temperature.

Figure 5: Conduction band of APL91.

Figure 6: Gain contours (a) and density of states (b) of APL91.

3 HIGH QCL OUTPUT USING SIMULATOR

3.1 Investigation of High Output by Simulation

Since it was found that the wavelength can be calculated accurately by our simulator as shown in Sec 2.2, we attempted to design a high-power active region for QCLs using this simulator. The design was based on the structure shown in Fig. 5 (Evans et al., 2007). The material is $Ga_{0.331}In_{0.669}As$ for the wells and $Al_{0.638}In_{0.362}As$ for the barriers. In this structure, one period consists of 22 layers, the injection region is from the 1st to 14th layers, and the active region is from the 15th to 22nd layers. The injection region is doped with 2.0×10^{16} cm^{-3} Si. Electrons are injected from the injection region into the upper subband of the active region, and they drop to the lower subband through the intersubband transition. Photoemission occurs at that time. This structure is denoted as APL91. Many cases were calculated while adjusting parameters related to net strain, calculation range, and convergence condition.

Figure 6 shows the gain contour diagram and DOS for APL91. The maximum gain of 91.33968 cm^{-1} with a photon energy of 260 meV (wavelength of 4.767 μm) can be seen in the second well of the active region (around the horizontal axis of -10, 40 nm) in the gain contour diagram. Since the experimental wavelength is 4.705 μm, the calculated value is in good agreement with the experimental one. In the DOS diagram, the DOS is larger in the well next to the thick barrier of the injection region. Electrons are injected from this well into the active region. In addition, large values of DOS are distributed in the upper and the lower subbands of the active region. Strong luminescence is generated by these DOS distributions.
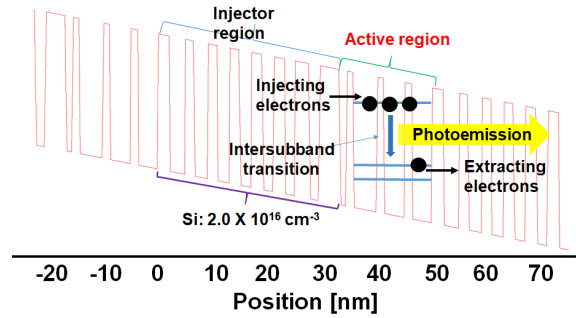
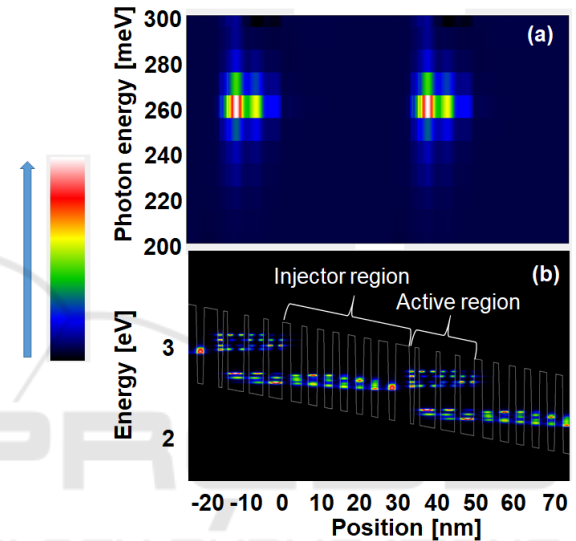First, simulations with various parameters were performed on the basis of physical considerations. The film structure with the noticeable change in gain was the structure in which the thicknesses of the barriers in the active region were varied. The calculated gains of this design are shown in Fig. 7.

When the barriers in the active region were made thinner, the gain increased, and a maximum gain that is 1.61 times that in APL91 was seen. On the other hand, in the structures in which the thicknesses of barriers are increased, the gains are lower than those in APL91.

High outputs can be expected from "the structure with thin barriers in the active region", but if the structure is markedly changed, fabricating the prototype becomes difficult. Figure 8 shows the net strain of the structures in which the barrier thicknesses of the active region are varied. Since the net strain increases as the thickness decreases, the wavelength was calculated for a structure with 10 % thinner barriers and a structure with 10 % thicker barriers.
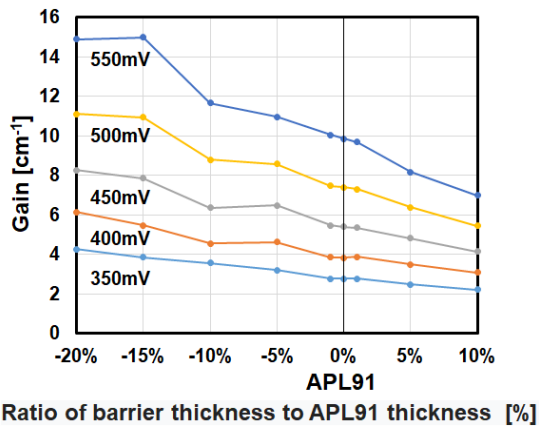
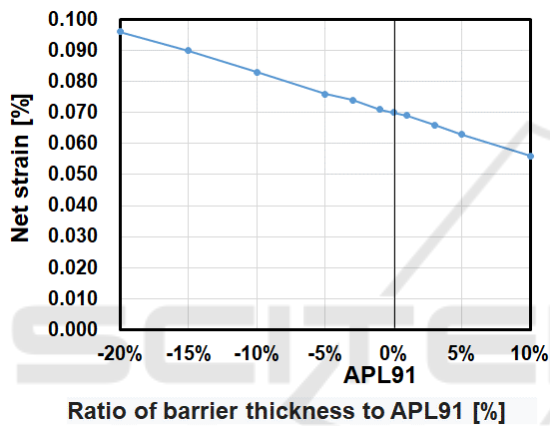Figure 7: Dependence of gain on barrier film thickness.

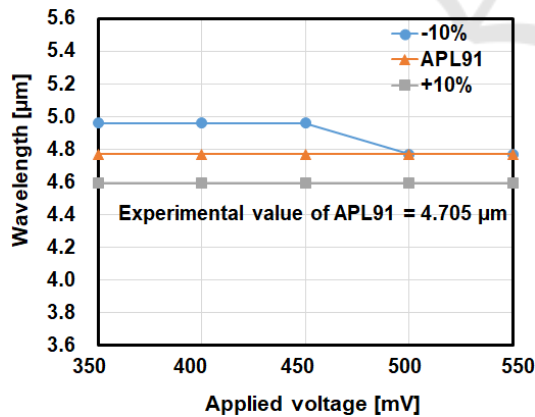Figure 8: Dependence of net stress on barrier film thickness.

Figure 9: Oscillation wavelength dependence on barrier film thickness.

Figure 9 shows the calculated wavelengths. The structure with 10% thinner barriers in the active region had a slightly longer wavelength than APL91. This is because the difference in energy between quantum levels contributing to photoemission

became narrow owing to the decreased thickness of the barriers. On the other hand, the wavelength was shortened in the structure with 10% thicker barriers in the active region, because the energy difference of the quantum levels that contributes to photoemission became wide with increasing thickness of the barriers in the active region.

3.2 Characteristics of Laser Output

On the basis of calculation results, we fabricated devices for measuring EL with 10 % thinner barriers (−10% device) in the active region. The device length is 4 mm and the ridge width is 15 μm. The device is mounted on an NS mount by In evaporation and flux without a submount. The device was operated at a frequency of 100 kHz, a pulse width of 300nm (duty 3%), and a cooling temperature of 273 K.

Figure 10 shows the EL spectra of the prototypes. The horizontal axis represents wavelength and the vertical axis represents EL intensity. Good emission was observed in the −10 % EL device. The emission wavelength is about 4.8 μm, which is in good agreement with the calculated value in Fig. 9. We also observed that the EL intensity of the −10 % device was 1.4 times that of APL91.
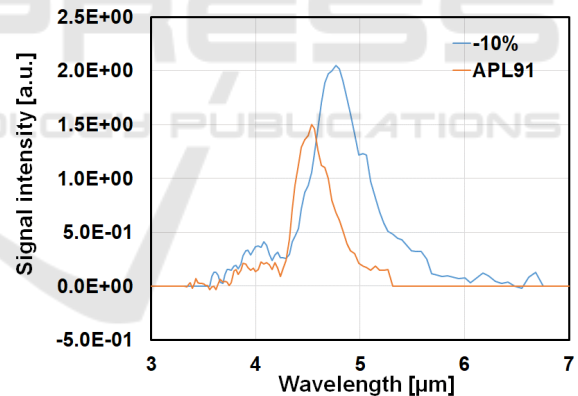

Figure 10: EL spectra of APL91 and prototype with 10 % thinner barriers.

4 CONCLUSIONS

We calculated the QCL wavelengths and the temperature dependence of the wavelength with a simulator using NEGF, and compared them with the experimental results reported in the literatures and our prototype QCLs. The difference between the oscillation wavelength of QCL and the oscillation wavelength obtained by the simulation was less than 0.36μm, and the wavelength dependences on the

active layer structure and the operating temperature were in good agreement with those obtained in the experiments in the references and those obtained with our QCLs.

Furthermore, the active layer was designed to increase the gain using a simulator, and it was shown that the output could be improved by reducing the barrier thicknesses in the active layer. We fabricated QCLs with this structure and evaluated their output wavelength and power. As a result, the EL emission intensity was increased to 1.4 times that of the previous structure QCL, and it was shown that the simulator design method is effective for the structure design of QCLs.

ACKNOWLEDGEMENTS

REFERENCES

Faist, J., Capasso, F., Sivco, D. L., Sirtori, C., Hutchinson, A., & Cho, A. Y. (1994). Quantum cascade laser. *Science*, 264, 553–556.

Jirauschek, C., & Kubis, T. (2014). Modeling techniques for quantum cascade lasers. *Appl. Phys. Rev.*, 1, 011307.

Grange, T. (2015). Contrasting influence of charged impurities on transport and gain in terahertz quantum cascade lasers. *Phys. Rev. B*, 92, 241306–31–5.

Kirch, D., Chang, C.-C., Boyle, C., Mawst, L. J., Lindberg, D., Earles, T., & Botez, D. (2015). Highly temperature insensitive, low threshold-current density (λ = 8.7–8.8 µm) quantum cascade lasers. *Appl. Phys. Lett.*, 106, 151106–1–5.

Yu, J. S., Slivken, S., & Razeghi, M. (2010). Injector doping level-dependent continuous-wave operation of InP-based QCLs at $\lambda \sim 7.3$ µm above room temperature. *Semicond. Sci. Technol.*, 25, 125015–1–5.

Wang, C. Y., Kuznetsova, L., Gkortsas, V. M., Diehl, L., Kärtner F. X., Belkin, M. A., Belyanin, A., Li, X., Ham, D., Schneider, H., Grant, P., Song, C. Y., Haffouz, S., Wasilewski, Z. R., Liu, H. C., & Capasso, F. (2009). Mode-locked pulses from mid-infrared quantum cascade lasers. *Opt. Express*, 17 (15), 12929–12943.

Faist, J., Capasso, F., Sirtori, C., Sivco, D. L., Baillargeon, J. N., Hutchinson, A. L., Chu, S. N. G., & Cho, A. Y. (1996). High power mid-infrared ($\lambda \sim 5$ µm) quantum cascade lasers operating above room temperature. *Appl. Phys. Lett.*, 68, 3680–3682.

Evans, A., Darvish, S. R., Slivken, S., Nguyen, J., Bai, Y., & Razeghi, M. (2007). Buried heterostructure quantum cascade lasers with high continuous-wave wall plug efficiency. *Appl. Phys. Lett.*, 91, 071101–1–3.

Faist, J., Capasso, F., Sivco, D. L., Hutchinson, A. L., Chu, S.-N. G., & Cho, A. Y. (1998). Short wavelength quantum cascade laser based on strained compensated InGaAs/AlInAs. *Appl. Phys. Lett.*, 72, 680–682.

Aldukhayel, A., Jin, S. R., Marko, I. P., Zhang, S. Y., Revin, D. G., Cockburn, J. W., & Sweeney, S. J. (2013). Investigations of carrier scattering into L-valley in λ = 3.5 µm InGaAs/AlAs(Sb) quantum cascade lasers using high hydrostatic pressure. *Phys. Status Solidi B*, 250 (4), 693–697.

Wen, Y., Quanyong, L., Wanfeng, L., Jinchuan, Z., Lijun, W., Junqi, L., Lu, L., Fengqi, L., & Zhanguo, W. (2011). Porous waveguide facilitated low divergence quantum cascade laser. *Semicond.*, 32 (6), 064008.